Flow-Tube Investigation of the High-Temperature Reaction between BCl_3 and NH_3

Anthony H. McDaniel and Mark D. Allendorf*

Combustion Research Facility, Sandia National Laboratories, Livermore, California 94551

Received: April 14, 1998; In Final Form: July 14, 1998

The reaction between BCl_3 and NH_3 to produce dichloroboramine (Cl_2BNH_2) and HCl was probed using a flow-tube reactor interfaced to a molecular-beam mass-sampling system. A composite method that couples the detailed simulation of the fluid mechanics and chemical reactions occurring in the flow tube to an algorithm for nonlinear least-squares optimization was used to extract the kinetic parameters from the experiment. The rate constant for this gas-phase reaction is k (cm^3 mol^{-1} s^{-1}) = 4.21×10^{11} exp[−(8350 cal mol^{-1})/(RT)] with an estimated uncertainty of 10−15% over the temperature range 670−920 K. The results indicate that surface reactions involving BCl_3 and NH_3 occur in the flow tube, but their contributions to the observed chemical behavior of the system can be quantified and therefore do not affect the kinetic measurements reported here. In addition, the low-energy barrier to this gas-phase reaction has important implications for the chemical vapor deposition of boron nitride from BCl_3 and NH_3.

I. Introduction

Chemical reactions between Lewis acid−base pairs such as BX_3 (X = H, F, Cl) and NH_3 are of fundamental importance and have been the subject of intense investigation.[1−5] The resulting complexes ($X_3B{:}NH_3$) are isoelectronic analogues of organic compounds (X_3CCH_3) but are unstable solids at room temperature that possess large dipole moments about the B:N center.[2,5] Furthermore, they readily eliminate HX to form X_2BNH_2.[6−8] It is these reactions that create a practical synthetic route to valuable III−V materials such as boron nitride (BN).

The desirable properties of BN, either in hexagonal or pyrolitic form, have been exploited in a variety of applications, including corrosion-resistant coatings and ceramic components,[9] debonding layers in ceramic-matrix composite materials,[10,11] and coatings on nuclear fuel elements.[12] In the majority of these applications, BN is deposited via chemical vapor deposition (CVD) processes in which the precursors of choice are boron trichloride and ammonia.[9] Despite the wealth of literature available on B−N coordination compounds, little is known about how BCl_3 and NH_3 are transformed into BN. In 1972, Kwon and McGee[13] reported that BCl_3 and NH_3 react at room temperature to form dichloroboramine:

$$BCl_3 + NH_3 \rightarrow Cl_2BNH_2 + HCl \qquad (1)$$

The reaction products were identified using time-of-flight mass spectrometry. No mass fragments unique to the $Cl_3B{:}NH_3$ adduct were observed, which is not surprising considering the difficulty reported by Avent et al.[8] in isolating this compound. Following Kwon and McGee's report, several other investigators have documented reaction 1.[14−16]

These observations cast doubt on the conclusions of several researchers who state that BN CVD is kinetically limited by the adsorption of BCl_3 or that homogeneous reactions are unimportant. Patibandla and Luthra[17] and Lee et al.[18] measured BN deposition rates and found an activation barrier of 35−40 kcal mol^{-1}. Although this value is consistent with other determinations cited by these investigators, their conclusions are based on measurement techniques that could not resolve the detailed process chemistry. The experiments of Kwon and McGee, Avent et al., and others suggest that little if any BCl_3 remains intact to adsorb at the growth front under the typical CVD conditions of excess NH_3 and temperatures exceeding 1000 K.

To complicate matters further, the dichloroboramine produced in reaction 1 is also a Lewis acid, albeit a weaker one than BCl_3 due to the presence of the less electronegative amino group. As is the case for BCl_3, NH_3 can donate electrons to the unfilled boron p-orbital, resulting in further amination:[16,19,20]

$$Cl_2BNH_2 + NH_3 \rightarrow ClB(NH_2)_2 + HCl \qquad (2)$$

$$ClB(NH_2)_2 + NH_3 \rightarrow B(NH_2)_3 + HCl \qquad (3)$$

This fact, coupled with the elimination of HCl from dichloroboramine,[16,19,20]

$$Cl_2BNH_2 \rightarrow ClBNH + HCl \qquad (4)$$

suggests that the gas-phase chemistry in this system is quite rich and deserving of a more detailed investigation. It seems likely that in many cases, BCl_3 is not the sole or even the most abundant boron-containing species that interacts with the BN surface during deposition.

In this investigation, a molecular-beam mass spectrometer (MBMS) sampling system interfaced to a high-temperature flow reactor (HTFR) was used to extract the kinetics of reaction 1 via a conventional discharge-flow approach. Traditional methods of data reduction have been replaced by a numerical procedure in which a detailed simulation of the fluid dynamics and chemistry in the flow reactor is coupled to a nonlinear least-squares algorithm. This procedure results in a direct determination of the kinetic parameters that govern the system. Comparison of our findings with the only other rate constant reported for reaction 1, that of Kapralova et al.,[15] indicates that

* Author to whom correspondence should be addressed. E-mail: mdallen@sandia.gov.

S1089-5639(98)01846-5 CCC: $15.00
Published on Web 09/15/1998

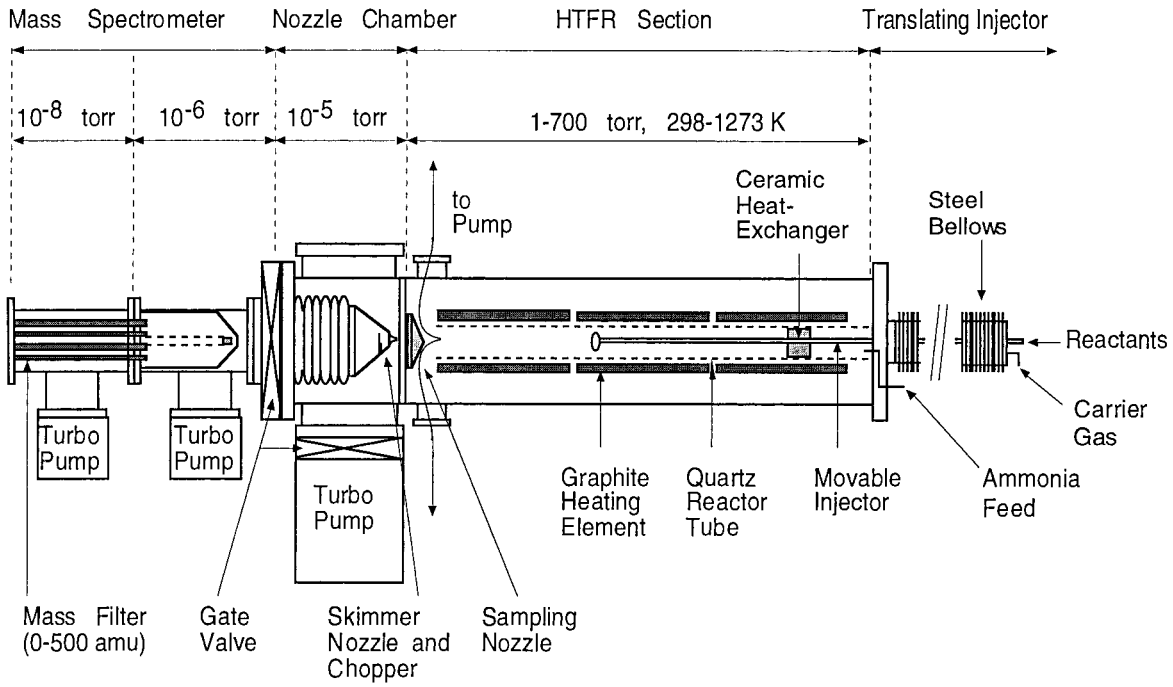

Figure 1. Schematic of high-temperature flow reactor (HTFR).

the gas-phase reaction between BCl_3 and NH_3 is much slower than previously thought.

II. Experiment

Apparatus and Measurements. The experimental apparatus is depicted in Figure 1 and consists of a high-temperature flow reactor interfaced to a molecular-beam mass spectrometer. The HTFR is a water-jacketed steel chamber that contains alumina- and graphite-felt insulation (not shown), heating elements, a flow tube, a ceramic heat exchanger, and a translating injector. The flow tube is constructed of quartz, has an internal diameter of 6.4 cm and an overall length of 112 cm, and is lined with 0.5 mm thick graphite foil to minimize deposition on the tube walls. Resistive heating elements encircle the tube, creating three independently controlled heating zones. The injector, also made of quartz, is mounted on a translating stage that is attached to the HTFR by a flexible metal bellows.

Mass flow controllers are used to meter all gas feed rates. Reactants are introduced into the flow tube via the injector and are dispersed at right angles to the axis of the tube by issuing through a sparger. Alternate feeds for ammonia and carrier gas are located at the entrance to the flow tube and at the top of the translating stage. The reactor exhaust is throttled, allowing for feedback control of the reactor pressure to any desired setpoint within the range 1−700 Torr. Power to each heating element is also under feedback control, using type-K thermocouples in contact with the outside wall of the flow tube. This results in a variation in the centerline temperature of ±2 K about the setpoint over the 30 cm length of the tube used to extract kinetic data. Residence times up to 2000 ms can be achieved by adjusting the injector position, gas flow rate, pressure, and temperature.

Gases exiting the flow tube are sampled using the technique of modulated molecular-beam mass spectrometry (MBMS). The sampling train consists of three differentially pumped vacuum stages (see Figure 1). The first chamber houses a 1500 L s^{-1} turbo pump, adjustable skimmer nozzle assembly, tuning fork chopper, and molecular-beam entrance aperture. The intermediate chamber, fitted with a 150 L s^{-1} turbo pump, further reduces the background pressure and serves to minimize beam scattering and transmission of off-beam gases into the third chamber. This final chamber houses an electron-impact ionizer, adjustable ion optics, a mass-spectrometer quadrupole assembly capable of unit resolution to 500 amu, and a conversion-dynode/electron-multiplier pair for detection of positive or negative ions (Extrel C50). The pressure in this chamber is maintained at $\sim 5 \times 10^{-8}$ Torr with a 400 L s^{-1} turbo pump.

The molecular beam originates in the first of the three vacuum stages as the reactor gases pass from a region of relatively high pressure ($P > 1$ Torr) to one of low pressure ($P_{max} < 2 \times 10^{-5}$ Torr), through the 125 μm diameter orifice in the sampling nozzle. The flow exiting the nozzle is supersonic and under-expanded. By maintenance of a background pressure in the first (expansion) chamber that is low enough to prevent continuum flow, complicating shock structures are avoided and the gas undergoes a smooth transition to free molecular flow.[21] Under these conditions, the expansion can be considered ideal and isentropic. Most importantly, within 2−5 nozzle diameters, the flow becomes rotationally cold and collisionless, which "freezes" the chemical composition of the mixture. This allows transient or short-lived species to be detected as well as stable compounds.[21,22]

Prior to electron-impact ionization at 70 eV, the molecular beam is chopped with a resonant modulator driven at 200 Hz. The chopper reference and analogue multiplier signals are routed through a lock-in amplifier (Stanford Research Systems SR510) where the modulated ion signals are extracted from the dc baseline. This allows for discrimination between beam gases and quiescent gases that are present in the quadrupole chamber. Phase-sensitive detection reduces the ultimate detection limit to less than 10 ppm at reactor pressures above 5 Torr in a helium carrier gas.

The reaction of BCl_3 with NH_3 was investigated at temperatures between 670 and 920 K in helium carrier gas at a reactor pressure of 10.0 ± 0.2 Torr. A few experiments were also performed with quartz wool inserted into the flow tube to determine the importance of wall reactions. Anhydrous ammonia (Scotty Specialty Gases 99.99 wt %), boron trichloride

(Matheson 99.9 wt %), and helium (Matheson 99.99%) were fed directly from their respective cylinders and were used without further purification. Unless indicated otherwise, the data presented here were collected under the following conditions: a total gas flow rate of either 1280 or 2000 sccm, an initial BCl_3 concentration of 2000 ppm, and a $[NH_3]/[BCl_3]$ ratio of 2.25, 3.0, or 4.5. Although unnecessary, given the new method of data reduction, ammonia was fed in excess to ensure first-order decay behavior of the BCl_3. A typical experimental run involved positioning the injector at five to ten different locations within the flow tube, recording the intensity of the desired ion signals at each position, changing the ammonia concentration or temperature, and then repeating the injector motion.

The reactants (BCl_3 and NH_3) were monitored by their respective parent-ion signals at mass/charge ratios (*m*/*e*) of 116 and 17. The product species, HCl, Cl_2BNH_2, and diaminochloroborane ($ClB(NH_2)_2$), were observed at *m*/*e* ratios of 36, 97, and 43, respectively. Mass flow controllers were used to calibrate the MBMS sampling system for BCl_3, NH_3, and HCl. Calibration factors for the two aminochloroborane species were calculated from the measured mass balances of hydrogen and chlorine. The reason for this choice, as opposed to basing the calibration on boron and/or nitrogen, is that compounds containing hydrogen and chlorine are least likely to be incorporated into solid deposits on the reactor walls before detection. The overall uncertainties in the reported species concentrations for BCl_3, NH_3, and HCl are estimated to be $\pm 5\%$. Those for the aminochloroborane compounds are higher.

An additional source of experimental uncertainty may arise from mass-discrimination-induced nonlinearities between the signal intensity and the absolute source density. This is especially severe for heavily seeded molecular beams of helium or hydrogen,[23] such as those used in flow-tube experiments. Therefore, to minimize the influence of mass discrimination, the source densities of reactants were kept small (less than 1% of the total feed) and all ion signals were normalized to an internal standard of argon (typically 2000 ppm). As a result, the mass-sampling system displayed a linear response to the concentrations of both reactant and product gases present in the exit stream of the flow tube under all experimental conditions.

Method of Analysis. In a standard flow-tube experiment, the injector position establishes the residence time for the reactants by fixing the distance between the detector and the point at which the primary and secondary reactants are mixed. Requisite data for a particular condition are collected by measuring the intensity of some signal that reflects the number density of the primary reactant as a function of the injector position. The kinetic parameters governing the transformation or decay of the measured signal can then be extracted from a solution to the steady-state transport equation for a single reaction in a cylindrical duct.[24,25] Given the complexity of a system where the chemistry and fluid dynamics are closely coupled, it becomes necessary to operate the experiment under limiting conditions so that data reduction and parameter extraction are simplified.

Various approximations and numerical procedures have been formulated in order to evaluate the transport equation, provided that certain experimental criteria are maintained.[26−28] Typically, the system must exhibit pseudo-first-order behavior in the decay of the primary reactant, usually accomplished by keeping the concentration of the secondary reactant in excess of the primary by an order of magnitude or more. Laminar flow conditions are usually adopted, with convective velocities large enough to negate axial diffusion. Secondary gas-phase reactions are neglected, and any heterogeneous chemistry must exhibit first-order behavior in the primary reactant with a well-determined rate constant that can be incorporated into the boundary conditions of the flow equation. Investigators often go to great lengths in order to satisfy these criteria so that simple approximations to the flow equation may be used to interpret experimental data.

Although it is fairly straightforward to maintain the flow conditions described above for reaction 1 and achieve pseudo-first-order behavior in the decay of BCl_3, secondary loss mechanisms due to gas-phase and surface reactions cannot be avoided. The product of the bimolecular reaction between BCl_3 and NH_3, dichloroboramine (Cl_2BNH_2), is a Lewis acid that further interacts with the NH_3 (reaction 2) and thereby decreases its concentration. More importantly, our results show that upon mixing, BCl_3 and NH_3 react at the surface, resulting in the loss of BCl_3 that cannot be quantified a priori. These additional reactions introduce an unacceptable level of uncertainty into the rate constant for reaction 1 obtained from standard flow-tube data-reduction techniques, thus requiring an alternative method for analysis and parameter recovery.

Here, we introduce a numerical method similar to the treatment of Segatz et al.[29] for calculating the kinetic constants from flow-tube data that does not rely on simplifications of the transport equations. A detailed model of the flow reactor has been coupled to an iterative procedure for parameter optimization to fit the experimental data to a predetermined reaction mechanism. The optimization program TJMAR1[30] minimizes the sum of squares of residuals, using the algorithm developed by Marquardt,[31] to arrive at a best estimate for the Arrhenius constants. TJMAR1 can solve both linear and nonlinear least-squares problems with weighted and constrained residual functions, which are formulated from the experimental data.

During the optimization, TJMAR1 recursively calls for the solution of the two-dimensional reacting-flow problem. To simulate the fluid dynamics and chemistry of the flow tube, we used the CRESLAF[32−34] and CHEMKIN[35,36] software packages. CRESLAF is a Fortran program that predicts the velocity, temperature, and species profiles in two-dimensional channels (planar or axisymmetric). The model uses a boundary-layer approximation to solve the coupled hydrodynamic and species continuity equations. As such, there must exist a principle flow direction in which convection dominates diffusive transport, a criteria that is always met under the laminar-flow conditions of these experiments. The model accounts for finite-rate gas-phase and surface chemistries, as well as multicomponent molecular transport, via the CHEMKIN, SURFACE CHEMKIN, and transport interpreters,[37] respectively. These three software packages compose a body of subroutines that are linked to CRESLAF, creating a standard deck from which to calculate equations of state, chemical production rates, thermodynamic properties, and mass diffusivities. For a complete discussion on CRESLAF and the CHEMKIN packages, the reader is referred to the above literature citations and the references therein.

The numerical treatment of the flow tube is enhanced by an accurate thermochemical database consisting of all participating species. Although not a strict requirement for the successful implementation of CRESLAF/TJMAR1, knowledge of the thermochemical properties (heats of formation, entropies, and heat capacities) allows for a more precise determination of the reverse reaction rates. For all compounds of interest except

NH_3, HCl, and He, the thermochemical properties were taken from the ab initio work of Allendorf and Melius.[20] In this data set, the results of ab initio electronic structure calculations, performed at the MP4(SDTQ) level of theory, were coupled with empirically derived bond-additivity corrections in order to predict thermochemical quantities. This method is known as the BAC-MP4 method (for bond-additivity-corrected fourth-order Møller−Plesset perturbation theory) and has been successfully applied to systems of first- and second-row compounds.[38,39] The data set we used encompasses 33 molecules in the B−N−Cl−H system and is believed to be the best and most complete available. Agreement between calculated heats of formation and those found in the literature is quite good (maximum error in the prediction less than ± 2.6 kcal mol^{-1}). For NH_3, HCl, and He, the requisite data were taken from the JANAF database.[40]

Basically, this composite method of reactor simulation and nonlinear least-squares optimization results in the direct determination of the kinetic parameters that govern the observed behavior, within the confines of the gas and surface reactions included in the model chemistry. This technique has two principal advantages over the highly specialized treatment reported by Segatz et al.[29] First, the CHEMKIN codes are designed as a general interface that facilitates the formulation, solution, and interpretation of problems involving elementary heterogeneous and gas-phase chemical kinetics in the presence of a solid surface. As such, with minimal effort, this method can be adapted to the study of different chemical systems in reactors of different geometries and flow/chemical complexities. Second, TJMAR1 allows for parameter optimization over weighted and constrained fields, which provides more flexibility in the extraction of rate coefficients.

As a result of the numerical treatment of the flow-tube data, traditional graphs of the rate constant verses inverse temperature or rate constant verses NH_3 concentration are not necessary. A benefit of manipulating data in this manner is that uncertainties in thermal uniformity within the tube and parasitic reactions that may occur in the gas-phase and on the surface of reactor walls are no longer a barrier to extracting meaningful rate constants from flow-tube reactors. Keys to the success of this method are a well-defined reaction mechanism and an appropriate choice of residual functions to minimize.

III. Results

HTFR Experiments. The reaction between BCl_3 and NH_3 was investigated at six temperatures between 670 and 920 K and at three initial mole fractions of NH_3 (4.5, 6.0, and 9.0 $\times$ 10^{-3}), which generated 18 separate conditions from which to collect rate data. Consistent with earlier investigations of this system,[13−16] we find that BCl_3 and NH_3 react rapidly over the entire range of temperatures examined. Three compounds were detected as products of the reaction: HCl, Cl_2BNH_2, and $ClB(NH_2)_2$. It is of interest to note that none of the previous investigators reported the presence of $ClB(NH_2)_2$, probably due to the lower reactor temperatures and/or lower instrument sensitivities employed in these studies.

Shown in Figure 2 are the first-order decay curves for the BCl_3 signal as a function of the relative residence time ($\tau - \tau_0$) for various initial $[NH_3]/[BCl_3]$ ratios at 670 K. Illustrated in Figure 3 are the decay curves measured at 918 K. The open symbols in these figures are the raw data with error limits established at the 95% confidence interval, and the solid lines are the results obtained from the CRESLAF/TJMAR1 analysis. The residence time relative to an initial injector position was

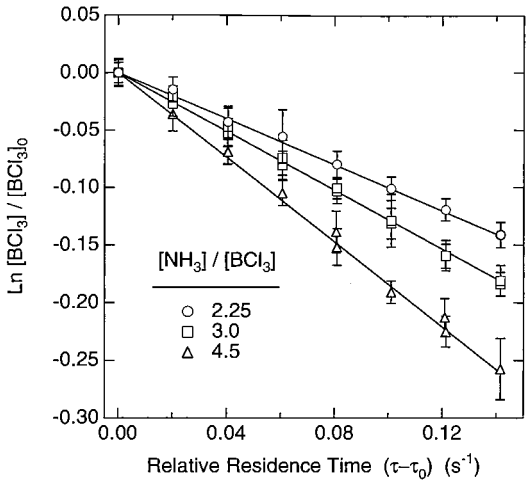

Figure 2. First-order decay of BCl_3 signal as a function of residence time for various feed ratios of $[NH_3]/[BCl_3]$ at 10 Torr and 670 K. Open symbols are data points with error limits at the 95% confidence interval; lines are the results of CRESLAF/TJMAR1 simulations (see text).

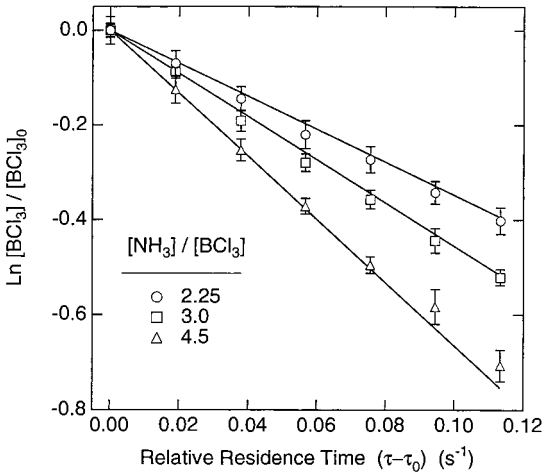

Figure 3. First-order decay of BCl_3 signal as a function of residence time for various feed ratios of $[NH_3]/[BCl_3]$ at 10 Torr and 918 K. Open symbols are data points with error limits at the 95% confidence interval; lines are the results of CRESLAF/TJMAR1 simulations (see text).

calculated according to $\tau - \tau_0 = (z - z_0)/\langle u \rangle$, where z (cm) is the physical distance between the injector tip and the sampling nozzle (see Figure 1), $\langle u \rangle$ (cm s^{-1}) is the average flow velocity, and the subscript (0) indicates the initial condition (injector position closest to detector). It is clear from these figures that the process is pseudo-first-order in the loss rate of BCl_3; it remains so under all conditions investigated.

While the curves in Figures 2 and 3 substantiate the first-order behavior of the process under study, this observation does not guarantee that the governing reaction is solely a homogeneous process. Both Brown[26] and Orkin et al.[28] report that a first-order wall loss would go undetected, meaning that the behavior of the system would remain linear, but have an observed slope that is steeper than that expected for a single gas-phase, bimolecular reaction. Therefore, to test for possible contamination of our observations by surface reactions, glass wool was placed in the flow tube. This increased the effective area exposed to BCl_3 and NH_3 by a factor of 70; any increase in the observed decay of the BCl_3 signal would immediately point to an active heterogeneous process.

TABLE 1: Mole Fractions of Reactant and Product Species for Various Conditions at a Residence Time of 0.5 s, 10 Torr, and 670 K

description			mole fraction ($\times 10^{-3}$)				
			measured ±5%[a]			simulated	
parent	ion	*m/e*	input	Δ_{LO}	Δ_{HI}	Δ_{SLO}	Δ_{SHI}
NH_3	NH_3^+	17	9.00	−1.37	−2.49	−1.18	−2.59
BCl_3	BCl_3^+	116	2.00	−1.13	−1.94	−1.08	−1.96
HCl	HCl^+	36	0.0	+1.11	+3.62	+1.21	+3.61
Cl_2BNH_2	$Cl_2BNH_2^+$	97	0.0	+1.01	+0.89	+0.94	+0.82
$ClB(NH_2)_2$	$B(NH_2)_2^+$	43	0.0	+0.09	+0.52	+0.05	+0.56

gas-phase atomic balance	input	difference (%)[b]		difference(%)	
		Δ_{LO}	Δ_{HI}	Δ_{SLO}	Δ_{SHI}
Cl	6.00	2.7	−1.9	1.5	1.3
B	2.00	1.4	26.3	4.2	29.1
N	9.00	2.0	6.2	1.4	7.2
H	27.0	2.3	0.0	0.8	1.0

[a] Uncertainties for Cl_2BNH_2 and $ClB(NH_2)_2$ have not been determined (see text). (+) indicates gain by reaction; (−) indicates loss by reaction. (Δ_{LO} = empty flow tube (low surface area), Δ_{HI} = glass-wool-packed tube (high surface area), Δ_{SLO} and Δ_{SHI} = results of CRESLAF/TJMAR1 simulation (see text). [b] Values are calculated by taking the percentage difference between the gas-phase mole fraction of the element in the input stream and that of the exit. A large positive value would indicate that the respective atomic element has been incorporated into a surface deposit.

The results of the experiment are presented in Table 1. Here, a comparison is made between the mole fractions of five species measured in the reactor, under identical flow conditions, with the exception that one set of data was obtained in an empty tube (low surface area) and the other in a glass-wool-filled tube (high surface area). The labels Δ_{LO} and Δ_{HI} represent empty- and filled-tube configurations, respectively. The Δ operator gives the difference between outlet and inlet mole fractions. As such, a "−" sign indicates that a species is consumed by the reaction, and a "+" indicates that a species is produced. Comparing Δ_{LO} and Δ_{HI} in Table 1 shows that the consumption of BCl_3 and NH_3 increases significantly at the higher surface area. Consequently, the production rates of HCl and $ClB(NH_2)_2$ increase; however, the amount of Cl_2BNH_2 decreases.

In the lower portion of Table 1, are the results of a mass balance over the flow tube for the elements (Cl, B, N, and H) detected in the gas phase. The values listed were calculated by taking the percentage difference between the mole fraction of the element in the input stream and that in the exit stream. Closure of the mass balance, within the experimental uncertainty, is achieved for the Δ_{LO} condition; however, for the Δ_{HI} state, the elements boron and nitrogen do not balance. The mole fraction of boron and nitrogen in the exit is much lower than in the input, which indicates that these two atoms have been removed from the gas phase, presumably incorporated into solid deposits on the surfaces within the reactor. The mole ratio of B/N lost to the surface is nearly 1:1, suggesting that stoichiometric BN is being formed.

Clearly, there is a heterogeneous component to the reaction between BCl_3 and NH_3. Given that the rate of this reaction cannot be determined a priori, it then becomes necessary to use an alternative approach to data reduction so that meaningful kinetic parameters can be extracted from the experiments. Posing a well-defined reaction mechanism is important for the success of the CRESLAF/TJMAR1 method. With the observations made in the empty and wool-filled reactor, we have sufficient information to develop a mechanism that describes the most significant reactions governing the chemistry of this system.

TABLE 2: Reaction Mechanism Used in the CRESLAF/TJMAR1 Calculations

reaction	*A*	β	*E* [a]
Gas[b]			
$BCl_3 + NH_3 \rightarrow Cl_2BNH_2 + HCl$	4.21×10^{11}	0.0	8350
$Cl_2BNH_2 + NH_3 \rightarrow ClB(NH_2)_2 + HCl$	3.88×10^{11}	0.0	18500
Surface[c]			
$NH_3 + * \rightarrow NH_3*$	5.00×10^{-2}	0.0	0
$3BCl_3 + 4NH_3* \rightarrow 6HCl + Cl_2BNH_2 + ClB(NH_2)_2 + BN(s) + 4*$	6.69×10^{-2}	−0.5	5240

[a] Units of cal mol^{-1}. [b] Gas-phase rate constant of the form $k = AT^{\beta} \exp[-E/(RT)]$ in (cm^3 mol^{-1} s^{-1}). [c] Surface-phase rate constant given as a sticking coefficient of the form $\gamma = AT^{\beta} \exp[-E/(RT)]$ which is unitless and in the range ($0 \le \gamma \le 1$). (*) indicates an adsorption site.

TABLE 3: Species Used in the Equilibrium Calculations

BCl_3	ClBNH	NH_3	He
$Cl_3B{:}NH_3$	$ClB(NH_2)_2$	NH_4Cl (s)	
Cl_2BNH_2	$B(NH_2)_3$	HCl	

Mechanism Development. The model chemistry used in the simulations is limited to the four reactions listed in Table 2. The two gas-phase steps, reactions 1 and 2, are discussed in the Introduction and are the subject of this investigation. Reactions 3 and 4 are not included in the mechanism because $B(NH_2)_3$ and ClBNH were never detected in the effluent of the flow tube. We also omit reactions describing the unimolecular decomposition of BCl_3 and NH_3 because these processes are highly activated and would not contribute to the gas-phase chemistry at the low temperatures and pressures employed in this investigation.[19]

For the surface, a simple two-step mechanism was devised to represent the interactions of NH_3 and BCl_3 at the gas−solid interface. This choice was based on the following experimental observations: upon addition of the glass wool (see Table 1, Δ_{HI}), there is an increase in the net loss of BCl_3 and NH_3, a concomitant increase in the production of HCl and $ClB(NH_2)_2$, and an unexpected decrease in the amount of Cl_2BNH_2 produced. No new gas-phase species were observed. There appear to be only two mechanisms consistent with these observations: (1) a surface reaction(s) that converts NH_3 and Cl_2BNH_2 to HCl and $ClB(NH_2)_2$ or (2) a surface reaction(s) that converts BCl_3 and NH_3 to the observed products. The first pathway, in principle, could deplete Cl_2BNH_2 and thereby drive reaction 1 in the forward direction, resulting in an increased rate of BCl_3 loss and a drop in the production of Cl_2BNH_2. However, this would be true only if reaction 1 were at equilibrium.

To test this hypothesis, equilibrium calculations were performed using the STANJAN code developed by Reynolds et al.[41] This program uses the method of "element potentials" to determine the equilibrium mole fractions of species in ideal mixtures of one or more phases. The species used in the equilibrium calculations are listed in Table 3. The molecules are all stable compounds and represent the most likely moieties to exist at the temperature and pressure investigated; no reactive intermediates were considered. Thermochemical data for all of the compounds except NH_4Cl(s), NH_3, HCl, and He were taken from the work of Allendorf and Melius described previously.[20] For the remaining species, the thermochemistry was again taken from JANAF.[40]

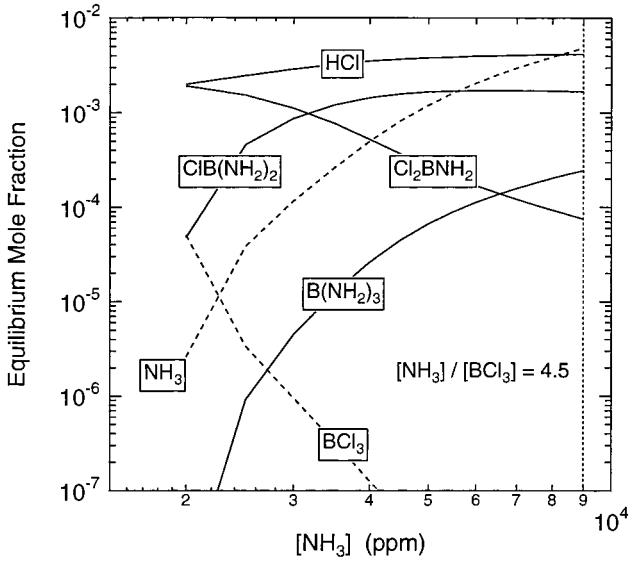

Figure 4. Equilibrium mole fractions for various species in the B−N−Cl−H system as a function of initial $[NH_3]$ at 10 Torr, 670 K, and an initial $[BCl_3] = 2000$ ppm. The vertical dashed line indicates the experimental condition.

Shown in Figure 4 are the predicted equilibrium mole fractions as a function of initial NH_3 concentration for a constant temperature (670 K) and pressure (10 Torr). At an $[NH_3]/[BCl_3]$ ratio of 4.5, which is similar to the experimental conditions for the data presented in Table 1, it is clear that Cl_2BNH_2 is not the most abundant product. Its equilibrium mole fraction is dwarfed by those of $ClB(NH_2)_2$ and $B(NH_2)_3$. The magnitude of the Cl_2BNH_2 concentration measured under the conditions of our flow-tube experiments shows that the system is far from equilibrium. Thus, the first mechanism described above is inconsistent with the equilibrium calculations. We therefore use the second mechanism and assume that NH_3 adsorbs on the surface with a high probability (i.e., relatively large sticking coefficient) and subsequently reacts with BCl_3 via a global process that results in the formation of gas-phase and solid products (see Table 2). To reduce the uncertainty associated with these uncharacterized surface kinetics, a single rate-limiting coefficient was chosen to represent the net reaction of BCl_3 at the wall. Although this global reaction does not describe the individual elementary processes that must occur, it will be shown later that it accurately predicts the behavior of the major gas-phase species under our experimental conditions.

The rate parameters listed in Table 2 are the final results of the analysis method and represent the optimal values, in a least-squares sense, of the kinetic constants. The (β) coefficients for temperature were held fixed, along with the preexponential factor (A) for the NH_3 adsorption step. The remaining six coefficients for the two gas-phase and global surface reactions were optimized to reproduce the experimental observations.

Nonlinear Least-Squares Analysis (CRESLAF/TJMAR1). As with most least-squares techniques, the total number of observations (N_{TOT}) should exceed the number of parameters (K). Here, we are interested in optimizing six rate coefficients for three reactions ($K = 6$). Experimental data, in the form of species concentration profiles, were collected under 18 different reactor conditions. In essence, every set of experimental conditions produced a concentration measurement for each of the five species listed in Table 1, at a multitude of injector positions. Therefore, the number of observations can be extended well beyond the number of experimental conditions, thus providing a sufficiently large set ($N_{TOT} > K$) from which to optimize the rate parameters. With reliable thermochemistry, a reaction mechanism, and a sufficient number of observations, the final step in parameter evaluation is to formulate the residual functions.

The residuals, which are cast into the form of relative errors and taken as the sum of squares, describe the extent to which the model predictions deviate from observation. In the interest of reasonable computation times, we decided to limit N_{TOT} to 36 data points. The most significant experimental results to fit are the family of decay curves for the BCl_3 signal (see Figures 2 and 3). Another observable that is sensitive to the rates of gas and surface reactions is the measured ratio of BCl_3 to Cl_2BNH_2. Given these two data sets, the sum of squares of residuals (SOR) for the first range (N_1) of 18 points, which represents the decay of BCl_3, is defined as:

$$\Phi_1 = \omega_1 \sum_{i=1}^{N_1} \left(1 - \frac{F_i}{Y_i}\right)^2 \tag{5}$$

$$F_i = \ln \frac{[BCl_3]_{i,1}}{[BCl_3]_{i,0}} \tag{6}$$

where Φ_1 is the SOR for range N_1, Y_i are the experimental values, which also take the form of eq 6, ω_1 is a weighting factor, N_1 is the number of data points within the range, and the subscripts (0 and 1) indicate the simulated value obtained for a reactor with the injector position fully forward (relative residence time of zero) or fully withdrawn (maximum relative residence time), respectively.

The SOR for the second range (N_2) of 18 data points, which is a measure of the $[BCl_3]/[Cl_2BNH_2]$ ratio in the exit stream, is given by

$$\Phi_2 = \omega_2 \sum_{j=1}^{N_2} \left(1 - \frac{F_j}{Y_j}\right)^2 \tag{7}$$

$$F_j = \frac{[BCl_3]_{j,1}}{[Cl_2BNH_2]_{j,1}} \tag{8}$$

where Φ_2 is the SOR for range N_2, Y_j are the experimental values in the form of eq 8, ω_2 is a weighting factor, N_2 is the number of data points within the range, and the subscript (1) indicates the simulated value obtained for a reactor with the injector position fully withdrawn (maximum relative residence time). The total SOR minimized by the program is the sum of eqs 5 and 7, $\Phi_{TOT} = \Phi_1 + \Phi_2$.

The objective of this work is to extract a reliable rate constant for the bimolecular reaction between BCl_3 and NH_3 (reaction 1). To this end, the SOR for range N_1 is given a much greater priority by the addition of a multiplicative weighting factor ($\omega_1 \gg 1$). An appropriate value for ω_1 was determined by increasing this factor until Φ_1 attained a minimum that was invariant to any further changes in the value of ω_1. This point represents the best possible fit to the measured decay characteristics of BCl_3. The robust nature of the numerical procedure is evidenced by the fact that the predicted pseudo-first-order rate constant (k, s^{-1}) for the decay of the BCl_3 signal does not vary by more than 2% in the range $1 \leq \omega_1 \leq 10^6$. However, the overall quality of the fit to the entire data set, represented by the value of Φ_{TOT}, is strongly influenced by this weighting factor due to the extreme sensitivity of eqs 7 and 8 to the four remaining rate parameters in the model chemistry. The best overall fit to the entire data set is obtained at values of ω_1 greater than 10^3.

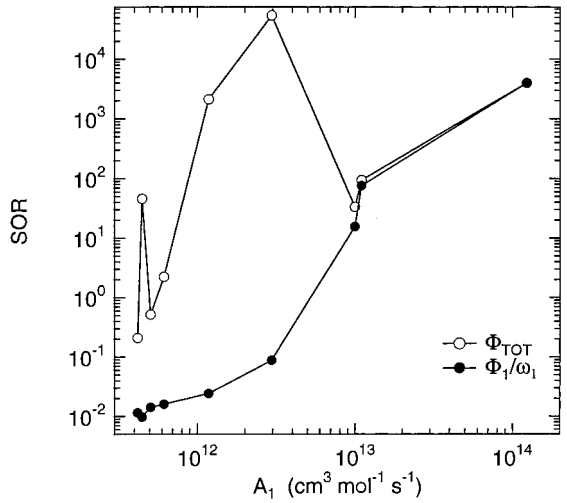

Figure 5. Sum of squares of residuals (SOR) plotted as a function of the preexponential factor for reaction 1. Open symbols are (Φ_{TOT}) which is the total SOR with the weighting factors removed; solid symbols are (Φ_1/ω_1) which is a partial SOR for the residuals defined in eq 5.

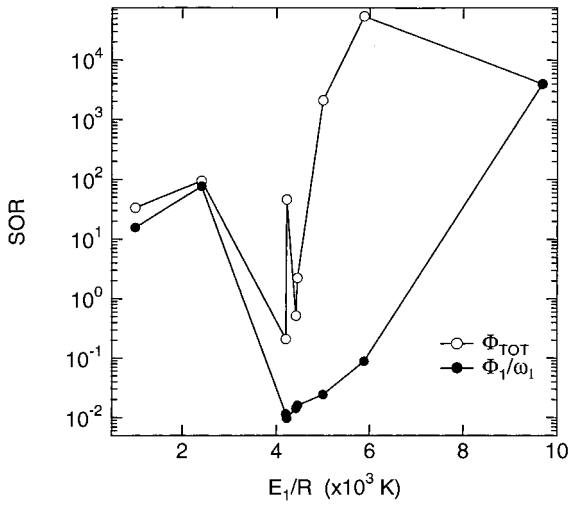

Figure 6. Sum of squares of residuals (SOR) plotted as a function of the activation energy for reaction 1. Open symbols are (Φ_{TOT}), which is the total SOR with the weighting factors removed; solid symbols are (Φ_1/ω_1), which is a partial SOR for the residuals defined in eq 5.

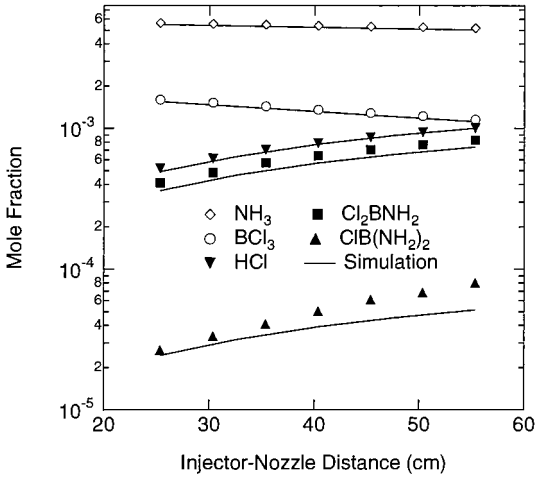

Figure 7. Species concentrations as a function of the injector-nozzle distance at 771 K, 10 Torr, an initial [BCl_3] = 2000 ppm, and an initial [NH_3] = 6000 ppm. Symbols are data points and solid lines are CRESLAF predictions using the full mechanism.

In addition to weighting the SOR for range N_1, the kinetic parameters were initially constrained to positive values within the range $10^{10}-10^{14}$ cm^3 mol^{-1} s^{-1} for the gas-phase preexponential factors, $(0.0-5.0) \times 10^4$ for activation energies (E_A/R in K), and 0.0−0.5 for the sticking coefficient prefactor. These constraints represent limits imposed upon the process by the stability of the numerical procedure but are quite consistent with the kinetics under investigation. For example, if the chosen rate of a reaction is unreasonably fast, the simulation will consume all of the BCl_3 within a very short distance from the reactor entrance. This leads to integration instabilities that result in excessively large values of Φ_{TOT} and premature termination of the program. In a typical numerical experiment, an initial guess for each of the six parameters was provided; the progress of the fit was then monitored by examining the value of Φ_{TOT}. Once a general pattern for the behavior of the solution space emerged, the initial guesses were given new values so that solutions could be approached from different points of origin. This was done to ensure that the optimized solution was not a local minimum.

Illustrated in Figure 5 are the SORs as a function of the prefactor value (A_1) for reaction 1. Similarly, in Figure 6 are the same SORs as a function of the activation energy (E_1/R) for reaction 1. The open symbols are values of Φ_{TOT}, with the weighting factors ω_1 and ω_2 removed ($\Phi_{TOT} = \Phi_1/\omega_1 + \Phi_2/\omega_2$), produced by the CRESLAF/TJMAR1 program for runs that had satisfied the exit criteria and were making no further progress in the reduction of Φ_{TOT}. The filled symbols are the corresponding values for Φ_1/ω_1. It is evident from Figures 5 and 6 that a deep well in the solution field for Φ_1/ω_1 emerges near the respective values of 4×10^{11} cm^3 mol^{-1} s^{-1} and 4.2×10^3 K. The existence of a unique minimum within the constrained ranges of the kinetic parameters is a good indication that a meaningful rate constant can be extracted with this technique. We should reiterate that Φ_{TOT} is a measure of the quality of the fit to the entire data set and is therefore dependent upon all six rate parameters associated with the model chemistry. Thus, small variations in (A_1) or (E_1/R) should not be interpreted as being responsible for large fluctuations in Φ_{TOT}.

For each value of Φ_{TOT} less than 10^2 in Figures 5 and 6, the convergence to a local minimum was usually attained in 10 or more iterations. At values of Φ_{TOT} greater than 10^2, the reactor simulations became unstable, causing the program to halt prematurely. Each iteration of the program required a minimum of N_{TOT} ($K + 1$) reactor simulations, resulting in an excess of 3000 complete reactor simulations per single run. Typical computation times were on order of 8 h on a Silicon Graphics Octane workstation.

To verify the accuracy of the model, predictions of species concentrations exiting the HTFR as a function of injector-nozzle distance were compared to experiment. Plotted in Figure 7 are the mole fractions that were measured and predicted for reactions occurring in an empty flow tube at 771 K, a [NH_3]/[BCl_3] ratio of 3.0, and a pressure of 10 Torr. There is excellent agreement between the CRESLAF/TJMAR1 results and the experimental data. The figure shows little discernible difference between the predicted and measured profiles (less than 5%) for NH_3, BCl_3, and HCl, which were the three compounds measured with the highest degree of accuracy. For the two remaining products, Cl_2BNH_2 and $ClB(NH_2)_2$, the model consistently underpredicts their rates of formation but not to a significant extent (maximum deviations of 10 and 36%, respectively). The quality of the fits is also evident in Figures 2 and 3 and the trends exhibited by the data in Table 1.

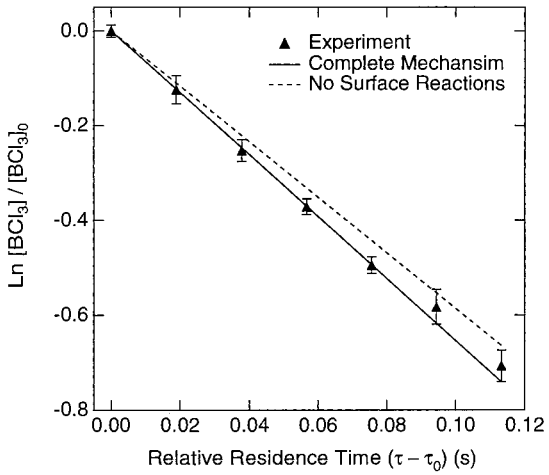

Figure 8. First-order decay of BCl_3 signal as a function of residence time at 10 Torr, a reactor temperature of 918 K, an initial $[BCl_3] = 2000$ ppm, and an initial $[NH_3] = 9000$ ppm. Solid symbols are data points with error limits at the 95% confidence interval; the solid line is the result of a CRESLAF simulation using the full mechanism; the broken line is the result of a CRESLAF simulation devoid of all surface reactions.

In Table 1, Δ_{LO} and Δ_{SLO} represent identical empty-tube configurations, with the former being experimental and the latter numerical. Similarly, Δ_{HI} and Δ_{SHI} represent packed-tube configurations. The model reproduces the increased consumption of BCl_3 as well as the increase in production of HCl and $ClB(NH_2)_2$ that is observed when the reactive surface is augmented by glass wool. Most noteworthy, however, is that the model predicts the observed decrease in the concentration of Cl_2BNH_2. This is an important subtlety that was not expected, given the single global surface reaction between BCl_3 and NH_3 that dictates the equimolar formation of BN(s), Cl_2BNH_2, and $ClB(NH_2)_2$. While it is unlikely that the two aminochloroborane species would be formed with equal probability on the walls, this result does indicate that the gas-phase concentration of Cl_2BNH_2 depends on a balance between the flux of BCl_3 to the surface and the rate of homogeneous reaction with NH_3.

The purpose of using CRESLAF/TJMAR1 to extract the kinetic parameters from the flow-tube data was to overcome the uncertainties associated with traditional methods of data reduction that are induced by secondary reactions occurring in the gas and on the surface of the reactor walls. With confidence in the predictive capabilities of the model, it can now be used to examine the relative effects of processes that may influence the concentration of BCl_3 exiting the HTFR. The first is reaction 2, which depletes the gas phase of both NH_3 and the byproduct of reaction 1 (Cl_2BNH_2), and the second is the surface reaction between BCl_3 and NH_3. We do this numerically by omitting these reactions and observing the effects on the simulated behavior of BCl_3. A reactor temperature of 918 K was chosen because these processes are activated and therefore would exert their greatest influence on the BCl_3 concentration at the highest temperature studied.

The gas-phase reaction between Cl_2BNH_2 and NH_3 has no observable effect on the decay of the BCl_3 signal. This process is highly activated and therefore is not a significant sink for NH_3; in fact, the surface is the major source of $ClB(NH_2)_2$. The heterogeneous reactions in Table 2, however, are a significant avenue for consumption of BCl_3. Illustrated in Figure 8 are two curves that represent the simulated first-order decay of the BCl_3 concentration as a function of relative residence time at an $[NH_3]/[BCl_3]$ ratio of 4.5 and a temperature of 918 K. All of the simulations are of the empty (i.e., low surface area) reactor tube. The top dashed line in this figure represents the model predictions for the gas-phase mechanism (reactions 1 and 2), omitting any surface chemistry. The solid line is the prediction resulting from the full mechanism; the solid symbols are data points with error limits at the 95% confidence interval. It is clear that the surface reactions increase the decay rate of BCl_3, since the slopes differ by more than 10%. Neglecting the bimolecular process between BCl_3 and NH_3 at the wall would result in a measured rate constant that is too large.

We conclude that the model chemistry proposed in Table 2 is valid for all experimental conditions examined in this work and that the composite method CRESLAF/TJMAR1 is an effective tool for extracting the kinetic parameters that govern the reactions. On the basis of the nonlinear least-squares analysis, the rate constant for reaction 1 is k (cm^3 mol^{-1} s^{-1}) $= 4.21 \times 10^{11} \exp[-(8350 \text{ cal mol}^{-1})/(RT)]$ with an estimated accuracy of 10−15%[24] over the temperature range 670−920 K.

IV. Discussion and Conclusions

Very few researchers have documented the reactions thus far considered, and only one has reported measuring a rate constant for reaction 1. Kapralova et al.,[15] working at significantly lower temperatures (345 K) than those used here, measured a rate near the collision frequency ($k = 6 \times 10^{12}$ cm^3 mol^{-1} s^{-1} at 10 Torr, 345 K). This determination is much faster than ours and is suspect because, at this low temperature, the concurrent deposition of solid NH_4Cl may open heterogeneous routes to BCl_3 decomposition. Unfortunately, Kapralova et al. do not provide sufficient detail in their paper to adequately evaluate their experiments. The authors only briefly describe the methods used to mix the reactants. The progress of reaction 1 was followed by mass spectrometry, but the authors do not state which mass peaks were monitored.

In their initial investigation, Kapralova et al. mixed nearly equal portions of BCl_3 and NH_3 in a small-diameter copper tube maintained at a temperature of 345 K and a pressure of 1−9 Torr. This technique is identical to that of Kwon and McGee,[13] who noted that solid formation was severe enough to clog the tube after only a few hours. Kapralova also concedes that heterogeneous reactions could not be avoided, so they adopted a more elaborate diffusion-flame approach. However, by keeping the reactor temperature well below the sublimation point of NH_4Cl ($T_{sub} = 613$ K), they could not prevent homogeneous nucleation of particles in the flow field upstream of their detector. To add to the uncertainty, Kapralova also describes a nonlinear, nonmonotonic pressure dependence of the reaction rate. This trend may be caused by pressure effects on the particle size distribution of aerosols formed within the reactor, which would in turn affect the rates of heterogeneous reactions, rather than by dependence of the bimolecular rate constant on pressure.

Kapralova's data also cannot be reconciled with theory. Ab initio calculations of the transition-state energetics using the BAC-MP4 method predict an energy barrier to reaction 1 equal to 13 kcal mol^{-1} at 298 K.[20] This value is 4.7 kcal mol^{-1} greater than the energy barrier determined experimentally, which is not surprising given the likelihood of significant ionic character in the transition state that cannot be accurately described by the basis sets employed by the BAC-MP4 method. Nevertheless, the experimental and theoretical evidence reported here suggests that a gas-phase reaction between BCl_3 and NH_3 does not approach the collision limit even at elevated CVD temperatures.

The energetics of reactions 2 and 3 follow the suppositions of both Allendorf and Melius[20] and Brink et al.[4] We observed

smaller quantities of $ClB(NH_2)_2$ than Cl_2BNH_2, indicating that reaction 2 is slower than reaction 1. The calculated energy barrier to reaction 2 is 10 kcal mol^{-1} greater than that of reaction 1, which is consistent with previous findings.[16,19] This behavior is expected as the strength of the Lewis acid decreases upon substitution of the NH_2 group for Cl. According to Brink et al., the ability of the Lewis acid to accept charge donated from the Lewis base, and thereby stabilize the resulting complex, will diminish as amino groups possessing smaller electron affinities replace the chlorines on boron. An extension of this argument to the limit of a fully aminated boron would imply that reaction 3 is slower still, which is reasonable considering that no $B(NH_2)_3$ was detected.

The results of this study indicate that both homogeneous and heterogeneous processes play important roles in BN CVD. The work reported by Patibandla and Luthra[17] and Lee et al.[18] implies that reaction 1 is not limiting to the rate of BN deposition, but this reaction likely plays an important role in determining the identity of the boron- and nitrogen-containing precursors that impinge on the growth front. Furthermore, since BN CVD typically involves high temperatures and excess NH_3, the subsequent reactions outlined in this paper will inevitably contribute to the formation of these precursors. While the exact sequence of reactions leading to BN formation from BCl_3 and NH_3 is still unknown, our findings create a platform for launching future investigations. Understanding the reactions of alternate species such as Cl_2BNH_2 or $ClB(NH_2)_2$ may provide the insight necessary to develop a full mechanism that in turn, could be used to develop and optimize BN CVD reactors.

The numerical technique developed here is well suited for the analysis of kinetic data collected in laminar-flow tubes. A benefit of using this composite method of simulation and nonlinear least-squares optimization is that thermal nonuniformity within the tube (radial and axial temperature gradients) and competing reactions that occur in the gas phase and at the surface are no longer road blocks to extracting meaningful rate constants from these reactors. In fact, it is not even necessary to collect data under pseudo-first-order conditions. This method is a tool that gives the researcher more latitude in the design and execution of flow-tube experiments. The example presented here does not fully establish the utility of such an approach, due to the limited influences of transport and surface chemistry on the bimolecular reaction between BCl_3 and NH_3. However, other experimental systems often encountered in the study of chemical vapor deposition reactions that occur at higher pressures or have more severe heterogeneous character would clearly benefit from this approach.

Acknowledgment. This work was supported by the U.S. Department of Energy, Office of Industrial Technologies, Advanced Industrial Materials Program.

References and Notes

(1) Zirz, C.; Ahlrichs, R. *J. Chem. Phys.* **1981**, *75*, 4980.
(2) Binkley, J. S.; Thorne, L. R. *J. Chem. Phys.* **1983**, *79*, 2932.
(3) Haaland, A. *Angew. Chem., Int. Ed. Engl.* **1989**, *28*, 992.
(4) Brink, T.; Murray, J. S.; Politzer, P. *Inorg. Chem.* **1993**, *32*, 2622.
(5) Jonas, V.; Frenking, G.; Reetz, M. T. *J. Am. Chem. Soc.* **1994**, *116*, 8741.
(6) Kroto, H. W.; McNaughton, D. *J. Chem. Soc., Dalton Trans.* **1985**, 1767.
(7) Legon, A. C.; Warner, H. E. *J. Chem. Soc., Chem. Commun.* **1991**, 1397.
(8) Avent, A. G.; Hitchcock, P. B.; Lappert, M. F.; Liu, D.-S.; Mignani, G.; Richard, C.; Roche, E. *J. Chem. Soc., Chem. Commun.* **1995**, 855.
(9) Paine, R. T.; Narula, C. K. *Chem. Rev.* **1990**, *90*, 73.
(10) Fareed, A. S.; Schiroky, G. H.; Kennedy, C. R. *Development of BN/SiC Duplex Fiber Coating for Fiber-Reinforced Alumina Matrix Composites Fabricated by Direct Metal Oxidation*; Proceedings of the 17th Annual Conference on Composites and Advanced Ceramic Materials, Cocoa Beach, FL, 1993.
(11) Cofer, C. G.; Economy, J.; Xu, Y.; Zangvil, A.; Lara-Curzio, E.; Ferber, M. K.; More, K. L. *Comput. Sci. Technol.* **1996**, *56*, 967.
(12) Gündüz, G.; Uslu, I.; Durmazuçar, H. H. *Nucl. Technol.* **1996**, *116*, 78.
(13) Kwon, C. T.; McGee, H. A., Jr. *Inorg. Chem.* **1973**, *12*, 696.
(14) Pavlovic', V.; Kötter, H.-R.; Meixner, C. *J. Mater. Res.* **1991**, *6*, 2393.
(15) Kapralova, G. A.; Suchkova, T. V.; Chaikin, A. M. *Mendeleev Commun.* **1993**, *3*, 118.
(16) Allendorf, M. D.; Osterheld, T. H. Chemical Reactions in the CVD of Boron Nitride from BCl_3 and NH_3. In *Proceedings of the XIII International Conference on Chemical Vapor Deposition*; Besmann, T. M., Allendorf, M. D., Robinson, M., Ulrich, R. K., Eds.; The Electrochemical Society Proceedings Series: Pennington, NJ, 1996; Vol. 96, p 16.
(17) Patibandla, N.; Luthra, K. L. *J. Electrochem. Soc.* **1992**, *139*, 3558.
(18) Lee, W. Y.; Lackey, W. J.; Agrawal, P. K. *J. Am. Ceram. Soc.* **1991**, *74*, 2642.
(19) Allendorf, M. D.; Melius, C. F.; Osterheld, T. H. A Model of the Gas-Phase Chemistry of Boron Nitride CVD from BCl_3 and NH_3. In *Covalent Ceramics III: Science and Technology of Non-Oxides*; Hepp, A. F., Kumta, P. N., Sullivan, J. J., Fischman, G. S., Kaloyeros, A. E., Eds.; Materials Research Society Symposium Proceedings 410; Boston, MA, 1996; p 459.
(20) Allendorf, M. D.; Melius, C. F. *J. Phys. Chem. A* **1997**, *101*, 2670.
(21) Miller, D. R. Free Jet Sources. In *Atomic and Molecular Beam Methods*; Scoles, G., Ed.; Oxford University Press: New York, 1988; Vol. 1, p 14.
(22) Knuth, E. L. Composition Distortion in MBMS Sampling. In *Applications of Free-Jet, Molecular Beam, Mass Spectrometric Sampling Proceedings*; National Technical Information Service, U.S. Department of Commerce: Springfield, VA (Distribution Code: UC-1400).
(23) Hsu, W. L.; Tung, D. M. *Rev. Sci. Instrum.* **1992**, *63*, 4138.
(24) Howard, C. J. *J. Phys. Chem.* **1979**, *83*, 3.
(25) Kaufman, F. *Science* **1985**, *230*, 393.
(26) Brown, R. L. *J. Res. Natl. Bur. Stand. (U.S.)* **1978**, *83*, 1.
(27) Walker, R. E. *Phys. Fluids* **1961**, *4*, 1211.
(28) Orkin, V. L.; Khamaganov, V. G.; Larin, I. K. *Int. J. Chem. Kinet.* **1993**, *25*, 67.
(29) Segatz, J.; Rannacher, R.; Wichmann, J.; Orlemann, T.; Dreier, T.; Wolfrum, J. *J. Phys. Chem.* **1996**, *100*, 9323.
(30) Jefferson, T. H. *TJMAR1-A Fortran Subroutine for Nonlinear Least Squares Prameter Estimation*; SLL-73-0305; Sandia National Laboratories: Albuquerque, NM, 1973.
(31) Marquardt, D. W. *J. Soc. Ind. Appl. Math.* **1963**, *11*, 431.
(32) Coltrin, M.; Kee, R. J.; Miller, J. A. *J. Electrochem. Soc.* **1984**, *131*, 425.
(33) Coltrin, M.; Kee, R. J.; Miller, J. A. *J. Electrochem. Soc.* **1986**, *133*, 1206.
(34) Coltrin, M. E.; Moffat, H. K.; Kee, R. J.; Rupley, F. M. *CRESLAF*: *A Fortran Program for Modeling Laminar, Chemically Reacting, Boundary-Layer Flow in Cylindrical or Planar Channels*, version 4.0; SAND93-0478 UC-401; Sandia National Laboratories: Albuquerque, NM, 1996.
(35) Coltrin, M. E.; Kee, R. J.; Rupley, F. M. *Int. J. Chem. Kinet.* **1991**, *23*, 1111.
(36) Coltrin, M. E.; Kee, R. J.; Rupley, F. M.; Meeks, E.; Miller, J. A. *Chemkin-III: A Fortran Chemical Kinetics Package for the Analysis of Gas-Phase Chemical and Plasma Kinetics; Surface Chemkin-III: A Fortran Package for Analyzing Heterogeneous Chemical Kinetics at a Solid-Surface—Gas-phase Interface*; SAND96-8216 UC-405 and SAND96-8217 UC-405; Sandia National Laboratories: Albuquerque, NM, 1996.
(37) Kee, R. J.; Dixon-Lewis, G.; Warnatz, J.; Coltrin, M. E.; Miller, J. A. *A Fortran Computer Code Package for the Evaluation of Gas-Phase Multicomponent Transport Properties*; SAND86-8246 UC-32, Sandia National Laboratories: Albuquerque, NM, 1986.
(38) Melius, C. F. BAC-MP4 Method. In *Chemistry and Physics of Energetic Materials*; Bulusu, S. N., Ed.; Kluwer Academic Publishers: Dorderecht, 1990; Vol. 309, p 21.
(39) Ho, P.; Melius, C. F. *J. Phys. Chem.* **1995**, *99*, 2166.
(40) Chase, M. W.; Davies, C. A.; Downey, J. R.; Frurip, D. J.; McDonald, R. A.; Szverud, A. N. *J. Phys. Chem. Ref. Data* **1985**, 14.
(41) Reynolds, W. C. *The Element Potential Method for Chemical Equilibrium Analysis: Implementation in the Interactive Program STANJAN*; Department of Mechanical Engineering, Stanford University, 1986.